Direct calibration of resistance thermometers between 10 K and 25 K by absolute acoustic gas thermometry in helium

PHILOSOPHICAL TRANSACTIONS A

royalsocietypublishing.org/journal/rsta

Research

Cite this article: Imbraguglio D, Steur PPM, Gavioso RM. 2026 Direct calibration of resistance thermometers between 10 K and 25 K by absolute acoustic gas thermometry in helium. *Phil. Trans. R. Soc. A* **384**: 20250043.
https://doi.org/10.1098/rsta.2025.0043

Received: 30 April 2025
Accepted: 14 July 2025

One contribution of 17 to a Theo Murphy meeting issue 'The redefined kelvin: progress and prospects'.

Subject Areas:
thermodynamics, acoustics, low temperature physics

Keywords:
thermodynamic calibration, absolute primary thermometry, acoustic gas thermometry, international temperature scale, capsule-type resistance thermometers

Author for correspondence:
Dario Imbraguglio
e-mail: d.imbraguglio@inrim.it

Electronic supplementary material is available online at https://doi.org/10.6084/m9.figshare.c.8153723.

THE ROYAL SOCIETY PUBLISHING

Direct calibration of resistance thermometers between 10 K and 25 K by absolute acoustic gas thermometry in helium

Dario Imbraguglio, Peter P. M. Steur and Roberto M. Gavioso

Istituto Nazionale di Ricerca Metrologica, Turin, Piedmont, Italy

DI, 0000-0002-1289-772X; RMG, 0000-0002-1631-5133

We have implemented absolute acoustic gas thermometry at 10 K, 13.8 K, 19 K and 24.6 K to evaluate the performance of this primary method for the direct thermodynamic calibration of capsule-type resistance thermometers, including both platinum and rhodium-iron types. Our implementation is based on speed of sound measurements in helium at a single pressure, chosen in the range 65 to 130 kPa, with non-ideality corrections relying on accurate *ab initio* calculations of the thermodynamic properties. The overall accuracy achieved in the determination of the thermodynamic temperature T varies between a minimum of 0.1 mK at 13.8 K to a maximum of 0.2 mK at 24.6 K. From the acoustic results and the calibration of thermometers on the international temperature scale ITS-90 providing T_{90}, we determined the differences (T–T_{90}), finding them in good agreement with the 2022 consensus estimates within the combined uncertainties. These results include a determination of the thermodynamic temperature at the triple point of neon T_{Ne} = (24.55502 ± 0.00030) K. This new value of T_{Ne} is consistent with other recent determinations obtained with various primary methods. Finally, we provide an example of a rapid, yet accurate, simplified thermodynamic calibration procedure.

This article is part of the Theo Murphy meeting issue 'The redefined kelvin: progress and prospects'.

1. Introduction

After more than one century of use for precise temperature metrology, resistance thermometers are still unsurpassed as the best performing and most practical devices for measuring temperature across wide ranges. For use in the cryogenic regime, special capsules filled with helium (He) are employed to ensure effective thermal contact between the external environment and the internal sensitive element; this is formed by a fine coiled wire made of either a highly pure metal or alloy, depending on the working temperature range. Capsule-type standard platinum resistance thermometers (CSPRTs) can cover the whole range from ambient temperature down to approximately 13.8 K. Below this threshold, CSPRTs are too insensitive and rhodium-iron resistance thermometers (RIRTs) are preferred owing to their superior sensitivity. In recent years, an alternative to RIRTs has appeared in the form of the platinum-cobalt (PtCo) thermometer. All these thermometers—with RIRTs and PtCo limited below 24.6 K—are conventionally calibrated on ITS-90 [1], which requires multiple measurements, for a complete calibration between 13.8 and 273.16 K, at eight pre-established fixed-point temperatures. Six out of eight fixed points are obtained through sealed cells, each one containing a different substance whereof the triple point is realized; no method currently exists allowing measurement of all of them by a single experimental apparatus. Therefore, thermometers are necessarily required to be mounted on customized adapters and moved from time to time into specific systems holding the cells; at least three independent measurements are required for the triple points of water, mercury and the cryogenic gases. In addition, the two remaining fixed points near 17 K and 20.3 K, i.e. the vapour-pressure points (VPPs) of equilibrium hydrogen, are typically no more realized with open cells or obtained using an interpolating gas thermometer (ICVGT), as prescribed by the ITS-90, but rather transferred with RIRTs [2] previously calibrated on an ICVGT. This procedure often requires additional comparison equipment for the subsequent and much more expeditious dissemination of multiple secondary calibrations at cryogenic temperatures. Consequently, in addition to all the risks and drawbacks associated with the transfers (e.g. mechanical shocks, workloads, etc.), primary calibrations of resistance thermometers on ITS-90 can take from several weeks to months, depending on the temperature range/subrange considered and the resulting number of fixed-point measurements required. More importantly, the main limitations of ITS-90 calibrations derive from the structure of ITS-90 itself, because of known errors in the values of thermodynamic temperature assigned to the defining fixed points, the restrictions coming from defined position and scarcity of calibration points along the range of validity, and non-uniqueness issues [3]. Recently, this limited perspective was modified by two relevant changes for temperature metrology: (i) the redefinition of the kelvin in 2019 [4], based on the assignment of an exact value to the Boltzmann constant k, accompanied by the *Mise en pratique* (*MeP*-K) with guidelines for its realization [5]; (ii) the accurate updated consensus estimate [6] of the differences between T and T_{90} below 335 K, from the determinations of thermodynamic temperature obtained by four gas-based primary thermometry methods, namely: acoustic (AGT), dielectric-constant (DCGT), constant-volume (CVGT) and refractive-index (RIGT).

The present work fits into this context to assess the performance and evaluate the uncertainty of AGT for the direct calibration of CSPRTs and RIRTs using thermodynamic temperature in the range 10 to 25 K. From previous ITS-90 calibrations of the same thermometers, the uncertainty in the realization of T and T_{90} is compared, and (T–T_{90}) differences are derived.

For all the results reported and discussed here, we implemented the absolute version of acoustic primary thermometry, which determines thermodynamic temperature T from an estimate of the speed of sound in He at zero pressure w_0 as

$$T = w_0^2 \frac{M}{\gamma_0 R}, \tag{1.1}$$

Table 1. Thermodynamic states investigated in this work, corresponding values of T and estimated standard uncertainties $u(T)$ determined from absolute AGT, values of T_{90} and estimated standard uncertainty $u(T_{90})$, resulting $(T–T_{90})$ differences and combined standard uncertainties $u(T–T_{90})$.

T_{ref}, p_{ref} (K, kPa)	$T \pm u(T)$ (K)	$T_{90} \pm u(T_{90})$ (K)	$(T–T_{90}) \pm u(T–T_{90})$ (mK)
10.0000, 66.640	10.000 141 ± 0.000 139	10.000 00 ± 0.000 42	0.14 ± 0.44
13.8033, 91.800	13.803 114 ± 0.000 110	13.803 30 ± 0.000 46	−0.19 ± 0.47
19.0000, 127.600	18.998 929 ± 0.000 170	19.000 00 ± 0.001 51	−1.07 ± 1.52
24.5561, 99.690	24.555 016 ± 0.000 202	24.556 10 ± 0.000 22	−1.08 ± 0.30
11 K, 77 kPa to 27 K, 185 kPa	NA	NA	see §3e

where M and γ_0 are, respectively, molar mass and ideal gas heat capacity ratios, and R is the molar gas constant. The value of R has been exactly defined since 2019 and entails no uncertainty contribution to AGT. Also, our investigated temperature range (10 to 24.5 K), being lower than the triple point of most ordinary gaseous substances, constrains the choice of the thermometric gas to He and facilitates an accurate estimate of the ratio M/γ_0. We assume γ_0 = 5/3 and M = 4.0026063 g mol^{-1} for our sample, and discuss below the validity of these assumptions, based on previous work with the same He batch [7]. He has the additional advantage that its thermodynamic properties are calculated from first-principles with very high accuracy. This is the case for the acoustic virial coefficients, which define the pressure dependence of the speed of sound w as a function of temperature:

$$w^2(T, p) = w_0^2(T)\left[1 + \omega_2(T)\frac{p}{RT} + \omega_3(T)\left(\frac{p}{RT}\right)^2 + \omega_4(T)\left(\frac{p}{RT}\right)^3 + \dots\right]. \tag{1.2}$$

In equation (1.2), $\omega_2(T) = \beta_a(T)$, $\omega_3(T) = RT\gamma_a{}^p(T)$ and $\omega_4(T) = (RT)^2\delta_a{}^p(T)$, where $\beta_a(T)$ is the second acoustic virial coefficient, and $\gamma_a{}^p(T)$, $\delta_a{}^p(T)$ are, respectively, the third and fourth acoustic pressure virial coefficients. We take advantage of the accuracy by which the acoustic virials of He $\beta_a(T)$, $\gamma_a{}^p(T)$, $\delta_a{}^p(T)$ are known from theory to calculate the correction expressed by the series in equation (1.2) as needed to experimentally determine w_0, and hence T, from speed of sound measurements $w(T_{ref}, p_{ref})$ taken in proximity of a single thermodynamic state nominally identified as (T_{ref}, p_{ref}), a procedure first demonstrated in [8] for a determination of the Boltzmann constant k. The reference values of pressure and temperature investigated in this work, listed in table 1, were chosen to be a close approximation to the realized thermodynamic conditions and, because in the course of the experiment the temperature of the gas is inferred by the readings of one or more thermometers calibrated on ITS-90, $T_{ref} = T_{90}$. At each state, our determinations of speed of sound are obtained by measuring the acoustic resonance frequencies f^{ac} of the radial modes of a He-filled copper cavity having quasi-spherical geometry and approximately 0.5 l internal volume. A precise estimate of the dimension of the cavity is obtained by measuring the microwave resonance frequencies f^{mw} of two transverse magnetic (TM) modes, upon correcting for the refractive index of He calculated from the polarizability and the dielectric virial coefficients predicted by *ab initio* calculations. Experimentally determined values of f^{ac} and f^{mw} must be corrected for major perturbing effects. Models of these corrections are available from the development of AGT supporting theory as reviewed in [9].

In the following sections, after a brief description of the most relevant features of the apparatus, we present and discuss the quality of the acoustic and microwave data. In both cases, this can be assessed by two main indicators, namely, the consistency of results obtained from different modes and the comparison between the modelled contributions to the resonance halfwidths with those determined experimentally. These indicators are then combined with

other minor contributions, including the uncertainty of the *ab initio* calculated properties of He, to define the overall uncertainty budget of our determination of T. In a separate section, we discuss the procedures used for the ITS-90 calibration of four capsule thermometers (two CSPRTs and two RIRTs) that were placed in contact with different parts of the resonant cavity. Unfortunately, temperature readings from the four capsules were not always found in agreement within their calibration uncertainty, with discrepancies particularly evident at 19 K (see §3d). These inconsistencies, which attest to the difficulty of ITS-90 calibration in the cryogenic range, severely limit the uncertainty of the (T–T_{90}) differences reported in this work (see table 1 and §3e).

Finally, to demonstrate the convenience of absolute AGT for direct thermodynamic calibration of capsule thermometers, we present and discuss the (T–T_{90}) results obtained by setting up a *fast* automated calibration procedure. In the course of the procedure, which determines T from the resonance frequency of a single acoustic mode, the He temperature and pressure within the cavity respectively vary along an isochore, between (11 K, 77 kPa) and (27 K, 185 kPa), providing 28 calibration points and requiring approximately 110 h to be completed.

2. Experimental method

(a) Overview of the apparatus

Speed of sound measurements in He were obtained using the apparatus previously developed in a microwave-only configuration to implement RIGT between 13.8 and 161.4 K [10]. Basically, it comprises a triaxial-ellipsoidal copper cavity (see figure 1), with 50 mm nominal internal radius, contained in a vacuum- and pressure-tight (up to 1 MPa) copper experimental vessel, itself surrounded by a vacuum-tight copper thermal switch vessel used to regulate heat transfer to the innermost stage of a pulse-tube cryocooler. Foil electrical heaters wrapped around the experimental and the thermal switch vessels can be used to set the working temperature in the range 9.5 to 300 K.

The experiment was adapted for the AGT measurements reported here with minor modifications, including flush mount with the internal surface of the resonator of two ¼″ free-field condenser microphones, located on the lower cavity hemisphere at positions labelled MP1 and MP2 in figure 1, to excite and detect the acoustic field. A copper tube with 0.8 mm internal diameter (not shown in figure 1) was inserted within a bored-through adapter on the cavity wall to form a gas inlet–outlet port with a total length of 50 mm. The port equilibrates the pressure within the cavity and the experimental vessel, which is connected by a dedicated gas line to the external manifold for regulation and measurement of the pressure based on the readings of a quartz transducer with a full-scale range of 690 kPa. The central conductor of two coaxial cables cut flush with the internal cavity surface act as very weakly coupled monopole antennas at positions MW1 and MW2 on the upper hemisphere.

A total of four T_{90}-calibrated capsule-type resistance thermometers, two CSPRTs and two RIRTs, were inserted into hollow posts bored within the resonator wall structure. CSPRTs with serial numbers RS144-01 and 5435 were placed at the top and bottom ends of the cavity, respectively, near RIRTs with serial numbers 200607 and 200609 (locations highlighted in figure 1). Details about the calibration history of the thermometers can be found in [2,10,11] and are discussed further below.

Coaxial and wiring connections from the microphones, the antennas and the thermometers lead, by suitable feed-through connectors, across the various stages of the cryostat to the instrumentation in the laboratory. With minor exceptions separately commented on below, instruments and devices were the same used for previous RIGT and AGT experiments, respectively described in [10] and in [7,12].

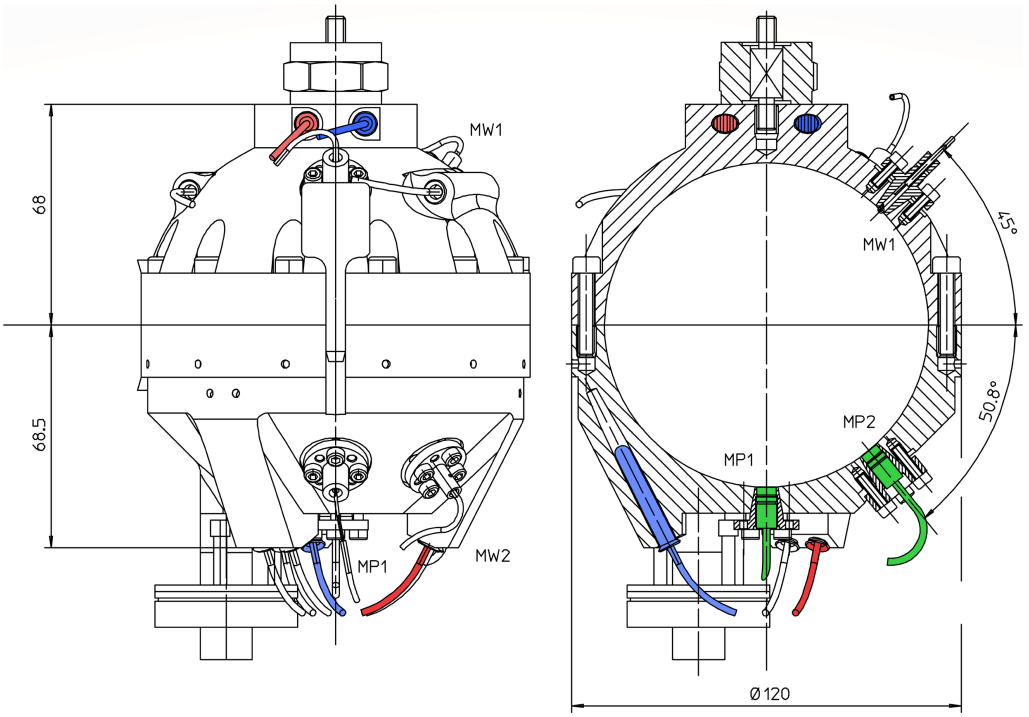

Figure 1. Front and cross-sectional schematic views of the AGT resonant cavity used in the present work, with dimensions in mm, showing the positions of microphones (MP1,2 in green), microwave antennas (MW1,2), platinum (CSPRTs in red) and rhodium-iron (RIRTs in blue) capsule resistance thermometers.

(b) Measurement procedure

The experiment was initially prepared by extensive evacuation of the different stages of the apparatus and by repeated flushing and filling with various samples of He, as needed for preliminary speed of sound measurements covering the overall temperature range 14 to 297 K for pressures up to 500 kPa. The results of these test measurements were useful to refine various aspects of the apparatus and measurement procedure; they are not reported on or further discussed here.

The temperature of the experiment was regulated by PID control of the current fed into a 230 Ω resistance foil heater wrapped around the external surface of the thermal-switch vessel, based on the readings of a thin-film resistance temperature sensor attached to its top head flange. During measurements, the thermal switch vessel was filled with a few mbar of He to increase and speed up heat transfer to and from the experimental vessel and the resonator contained therein. Heating power in the order of 3.5 W was sufficient to maintain the temperature of the experiment at 30 K. This simple temperature regulating system allowed for temperature stability of the experiment better than 0.1 mK over several hours. No pressure regulation or gas flow was implemented for this work, but temperature control normally maintained pressure fluctuations within ± 1 Pa of their mean.

Using the same instrumentation and fitting procedures described in [7,10,12], for each single experimental run at (T_i, p_i), the acquisition of a dataset composed by the resonance frequencies $f_{(0,N)}(T_i, p_i)$ and halfwidths $g_{(0,N)}(T_i, p_i)$ of eight radial acoustic modes, (0,2) to (0,9), and by the mean resonance frequencies $\langle f_{\mathrm{TM1}N}(T_i, p_i)\rangle$ and halfwidths $\langle g_{\mathrm{TM1}N}(T_i, p_i)\rangle$ of the triply degenerate microwave TM11 and TM12 modes, required approximately 17 min, and was repeated over a period of time lasting between a minimum of 3.5 h and a maximum of 12.5 h. From these records, each successively fitted frequency $f_i(T_i, p_i)$ is corrected to $f_i(T_{\mathrm{ref}}, p_{\mathrm{ref}})$, at the nominal reference temperature and pressure for the corresponding experimental run.

For both acoustic and microwave frequencies, these corrections—implemented as per eqns. (8) and (10) in [12]—require an estimate of the linear thermal expansion coefficient α_{th} of copper. In addition, the microwave and acoustic corrections involve, respectively, the refractive index $n(T, p)$ and the speed of sound $w(T, p)$ of He. Because the corrections are small, knowledge of all these quantities does not need to be accurate. However, for the cavity used here, accurate knowledge of α_{th} is available from previous microwave measurements in vacuum at different temperatures [10]. Also, as further discussed below, both $n(T, p)$ and $w(T, p)$ of He can be accurately calculated from first-principles. Once corrected, repeated measurements $f_i(T_{ref}, p_{ref})$ are averaged to provide a single mean estimate $f(T_{ref}, p_{ref})$. The standard deviation of this mean incorporates the uncertainty contributions arising from fitting single resonances, the stability and repeatability of the experiment, and the effectiveness of the corrections. For the acoustic measurements at 13.8 K, 19 K and 24.6 K, this uncertainty estimator was found negligibly small, relatively less than 0.3 ppm. Acoustic measurements at 10 K represented an exception, presumably because temperature control was not active, with the relative standard deviation of the mean of the frequency of several radial modes as large as 5 ppm. This exception was accounted for with a specific uncertainty contribution (row 1 in the uncertainty budget table 2) for the final estimate of T listed in table 1.

3. Results and discussion

(a) Acoustic model and corrections

For each radial acoustic mode (0,N), our determination of the speed of sound at the reference conditions $w_N(T_{ref}, p_{ref})$ from the corresponding measured resonance frequency $f_N(T_{ref}, p_{ref})$ is based on

$$w_N(T_{ref}, p_{ref}) = \frac{2\pi a(T_{ref}, p_{ref})}{z_{EN}}\left[f_N(T_{ref}, p_{ref}) - \sum \Delta f_N\right]. \tag{3.1}$$

In equation (3.1), the radius of the cavity at the reference conditions $a(T_{ref}, p_{ref})$ is determined from measurements of microwave resonances of the gas-filled cavity, as discussed below. The same measurements precisely determine the shape of the internal geometry by the shape parameters ε_1 and ε_2 which define the difference between the three semi-axes of the ellipsoid, namely, a, $a(1+\varepsilon_1)$ and $a(1+\varepsilon_2)$. Based on these parameters, corrections to the acoustic eigenvalues of a perfect sphere can be calculated [13] leading to precise estimates of z_{EN}. For our cavity, these corrections vary between a minimum of 0.5 ppm for mode (0,2) to a maximum of 18 ppm for mode (0,9).

Because of the interaction of the acoustic field within the cavity with the finite, non-uniform impedance of its internal cavity surface, the measured resonance frequencies $f_N(T_{ref}, p_{ref})$ must be corrected to account for the resulting perturbations, summarized by the summation symbol in equation (3.1). The interaction at the cavity surface, and to a minor extent within the bulk of the fluid, dissipates acoustic energy in a measure quantified by the resonance halfwidths $g_N(T_{ref}, p_{ref})$. Because experimental estimates of the halfwidths are obtained by fitting the resonance curves, and are otherwise calculable from theoretical models in a fully independent manner, the comparison of experimental and theoretical halfwidths is a reliable quantitative indicator of the completeness and adequateness of the acoustic model, proving that relevant perturbations have indeed been taken into account. In our modelled corrections to the experimental frequencies, we first account for perturbations induced by the thermal boundary layer, including the propagation of a thermo-elastic wave into the shell and imperfect thermal accommodation at the boundary. Calculation of these corrections requires an estimate of several thermophysical properties. At the thermodynamic conditions investigated here, thermal boundary corrections are small, overall ranging between −100 ppm for mode (0,2) at 25 K and −30 ppm for mode (0,9) at 10 K. Also, for He, thermophysical properties are accurately

Table 2. Uncertainty budget for the acoustic determination of the thermodynamic temperature *T*.

reference temperature/K		24.5561	19.0000	13.8033	10.0000
reference pressure/kPa		99.98	127.60	91.80	66.64
row	uncertainty source	relative standard uncertainty $u_r(T)$/ppm			
1	standard deviation of the mean of repeated measurements	0.37	0.45	0.48	8.18
2	thermal accommodation correction	0.41	0.26	0.22	0.20
3	shell correction	1.59	1.89	1.16	0.30
4	imperfect determination of pressure	1.83	1.68	0.22	3.50
5	maximum difference between selected modes	3.71	2.79	2.83	7.00
6	mean double excess halfwidth	6.61	7.62	6.52	6.64
	total acoustic	**7.98**	**8.52**	**7.22**	**13.1**
7	squared microwave radius resistivity	1.16	1.20	1.24	1.24
8	squared microwave radius total mode difference	1.42	1.42	1.42	1.42
	total microwave	**1.83**	**1.86**	**1.89**	**1.89**
9	***ab initio* correction to zero pressure**	**0.81**	**2.00**	**2.83**	**4.30**
	combined/ppm	**8.22**	**8.94**	**7.98**	**13.9**
		standard uncertainty $u(T)$/mK			
	combined/mK	**0.20**	**0.17**	**0.11**	**0.14**

known from theory [14] and contribute negligible uncertainty. The thermal accommodation correction varies between 0.6 ppm and 1.1 ppm, assuming the accommodation coefficient *h* to be comprised between 0.34 and 0.39 [15] at all investigated temperatures. The uncertainty contribution from the imperfect estimate of *h* is always less than 0.4 ppm and included only for completeness (see row 2 in table 2).

We account for the perturbation induced by the gas inlet–outlet duct by a calculation of its complex acoustic impedance [16]. The corresponding relative frequency perturbation was always less than 0.35 ppm, the relative contribution to the halfwidths was always less than 0.5 ppm. The real acoustic impedance of the diaphragm of two ¼″ condenser microphones, and the corresponding frequency perturbation, was calculated equal to −0.9 ppm for all modes and temperatures in this work, using eqn. (2.37) in [17]. Thus, the overall frequency perturbations induced by the duct and the acoustic transducers are small enough that their uncertainty contribution to the overall uncertainty can be neglected.

Finally, we considered frequency corrections as needed to account for coupling of the acoustic field within the cavity with elastic motion of the shell. In principle, larger perturbations to the acoustic radial modes are expected near the lowest radially symmetric mode of the shell, identified by a *breathing* frequency f_{br}, which can be calculated by analytical models. Experimental practice shows that the convoluted structure of a resonator differs enough from a simple isotropic spherical shell that coupling with non-radial modes of the shell may also be effective. For our cavity, a calculation based on the analytical model [18], and the elastic properties of copper, leads to an estimated f_{br} of approximately 20 kHz. However, our experimental observations evidence major perturbating effects taking place around 17.5 kHz. These observations are favoured by the large relative shift, by a factor 1.6, of the resonance frequencies as a consequence of the temperature increase between 10 and 25.4 K, with f_{02} varying between 2.7 kHz and 4.2 kHz and f_{09} varying between 15.8 kHz and 24.9 kHz. For instance, the dispersion and excess halfwidth plots in figure 2 show a large perturbation for mode (0,7) falling near 16.7

kHz at 19 K. Assuming f_{br} = 17.5 kHz, we used the simplified model of eqn. (3.1) in [17] to calculate corrections to the radial modes at different temperatures, typically found in the order of ± 5 ppm but rising to −40 ppm for mode (0,7) at 19 K. Our selection criteria of the best modes for the final determination of T reject modes with calculated shell perturbations larger than 10 ppm. While it is hard to work out a realistic estimate of the uncertainty of our educated guess of f_{br}, we conservatively assume 500 Hz as the standard uncertainty and estimate its contribution to the uncertainty by the difference between our determination of T upon recalculating shell corrections with f_{br} = 17 kHz or with f_{br} = 18 kHz (row 4 in table 2). If shell perturbations were ignored and no shell correction applied, the overall effect on T would vary between a minimum of 2.3 ppm at 24.5 K and a maximum of 8.2 ppm at 19 K.

The left-hand plot in figure 2 shows the progressive effect of applying successive corrections to the experimental acoustic frequencies measured at 19 K to account for various types of perturbations. Displayed are the corresponding (T–T_{90}) differences scaled in mK temperature units. Formally, the calculation of T in this plot requires the estimate of the cavity radius and the *ab initio* correction of the speed of sound at zero pressure, as discussed in the following sections. The right-hand plot in figure 2 shows the relative double excess halfwidths $2(g_{exp}-g_{calc})/f_{calc}$ scaled in mK for the same data. The large shell perturbation for mode (0,7) falling near our estimated breathing frequency of the shell is evident. Figure 3 shows the dispersion and excess halfwidth plots, scaled in mK units for acoustic data measured at other temperatures investigated here: 10 K, 13.8033 K and 24.5561 K.

For modes (0,2) to (0,7) at the four temperatures investigated here (with the exception of mode (0,7) at 19 K which is strongly perturbed by shell coupling), figure 4 plots the (double) relative excess halfwidths in ppm, $2(g_{exp}- g_{calc})/f_{calc}$, as a function of the corresponding mode eigenvalue. The clearly evident mode-dependent pattern indicates that our acoustic model is imperfect or incorrect in accounting for some perturbations, probably arising from the impedance of ducts and/or transducers. These observations suggest accounting for this imperfection with a specific uncertainty contribution as per row 6 in table 2.

(b) Microwave determination of the cavity radius

We estimate the internal radius of the cavity at the reference conditions $a(T_{ref}, p_{ref})$, and the shape parameters which define the acoustic eigenvalues z_{EN} in equation (3.1), from measurements of the resonance frequencies of the TM11 and TM12 electromagnetic modes falling, respectively, near 2.6 GHz and 5.8 GHz. In the temperature range explored here, the electrical resistivity of copper is in the order of 1.2 nΩ m, leading to resonance quality factors of approximately 1×10^5 and 1.7×10^5, and resonance halfwidths of 14 kHz and 17 kHz, for modes TM11 and TM12, respectively. For both modes, the standard deviation of repeated measurements is typically less than 0.01 ppm. Because microwave measurements take place while He fills the cavity, the estimate of the cavity radius at the reference conditions requires that the mode frequencies are first corrected by multiplication with the refractive index of the gas $n(T_{ref}, p_{ref})$. At 10 K and 66.64 kPa, n differs from unity by approximately 634 ppm, at 24.5 K and 100 kPa, by approximately 380 ppm. The calculation of $n(T, p)$ enjoys the progress achieved by theory in modelling the required electromagnetic properties of He, including the molar polarizability A_ε = 0.517 254 08(5) cm^3 mol^{-1} [19], the second dielectric virial coefficient B_ε (T) [20], for instance B_ε (10 K) = −3.9(1) cm^6 mol^{-2}, the third dielectric virial coefficient C_ε (T) [21], for instance C_ε (10 K) = −0.210(3) cm^9 mol^{-3}, and the diamagnetic susceptibility χ_0 = −1.891 04(3)×10^{-6} cm^3 mol^{-1} [22], with the number in brackets indicating the standard uncertainty of the last reported digit. Given the remarkable accuracy of these calculated properties, the uncertainty contribution of the correction by $n(T_{ref}, p_{ref})$ to our determination of $a(T_{ref}, p_{ref})$ and hence of T, is negligible. However, the refractive index is sensitive to small changes of density, like those possibly caused by errors in the experimental determination of T and p. At the densities explored here, an error of 100 Pa would change n by approximately 1 ppm,

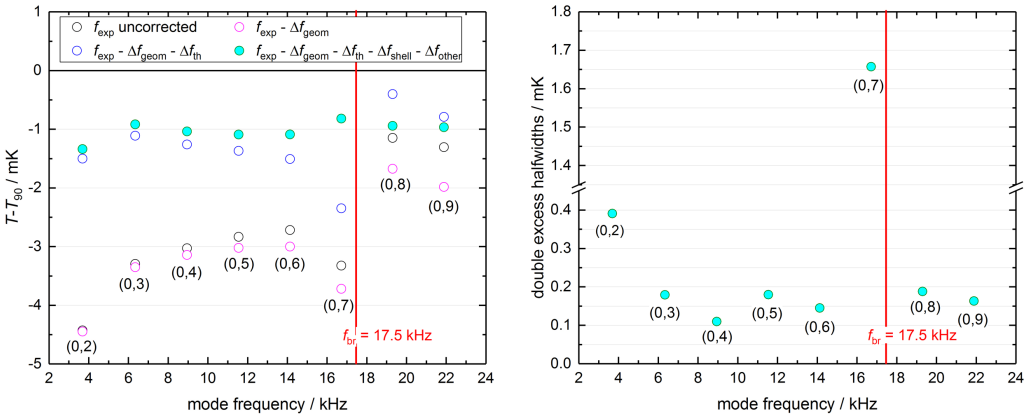

Figure 2. (Left) Progressive reduction of the dispersion of (T−T_{90}) results determined from eight radial acoustic modes measured at $T_{ref} = T_{90} = 19$ K upon successively subtracting from the experimental data corrections to account for various perturbations, that is, for the ellipsoidal shape of the cavity, for the thermal boundary layer, for the shell coupling and for the duct and microphone impedance. (Right) Double excess halfwidths, scaled in mK temperature units, $2T_{ref}(g_{exp} - g_{calc})/f_{calc}$ of acoustic resonances at 19 K. The plots evidence the larger perturbation occurring for mode (0,7) near the breathing frequency of the shell.

the same change would be caused by a temperature error of 15 mK. Both these sensitivities are low enough that their uncertainty contributions can be safely ignored. As for the acoustic modes, corrections to the experimentally measured resonance frequencies must be applied. A geometrical correction to the microwave eigenvalues of a perfect sphere, to account for the ellipsoidal shape of the cavity, can be calculated using the model in [23], based on the shape parameters determined from the relative separation of the single components of the modes, leading to ε_1 = (1.0592 ± 0.0004) × 10^{-3} and ε_2 = (0.50567 ± 0.0004) × 10^{-3}, at all temperatures investigated here, with relative corresponding corrections of 0.15 ppm and 0.89 ppm to the eigenvalues of TM11 and TM12, respectively. The finite electrical conductivity of the cavity surface allows for penetration of the field within the wall at the boundary with a major contribution to the resonance halfwidths and decreasing the frequencies by the same amount. Because we have no other modelled contributions to energy losses, correcting the experimental frequencies by adding the fitted mode halfwidths accounts for this perturbation. Alternatively, copper resistivity values can be obtained by fitting the resonance halfwidths, typically obtaining slightly different results from different modes. The change in the corrected frequencies resulting by these alternatives contributes to the uncertainty of our determination of the cavity radius with a relative contribution of 0.6 ppm, and twice as much to the determination of T (see row 7 in table 2). Additional small corrections are applied to account for the perturbations induced by the coaxial waveguides used as antennas, and the gas inlet–outlet duct, using the model in [24]. Upon these corrections, the radius calculated from modes TM11 and TM12 is compared and found to differ by 0.7 ppm, very nearly constant at all temperatures. This discrepancy is accounted for with a specific contribution (row 8 in table 2) of approximately 1.4 ppm to the uncertainty of T.

(c) Determination of thermodynamic temperature

The corrected unperturbed acoustic frequencies and the determination of the cavity radius at the reference conditions, discussed in the previous sections, lead to an estimate of the speed of sound $w_N(T_{ref}, p_{ref})$ for each radial mode. Before thermodynamic temperature can be calculated from these estimates, they must be corrected to corresponding values at zero-pressure. This correction is large, for instance at 10 K and 66 kPa $[w_N(T_{ref}, p_{ref})/w_N(T_{ref}) - 1]$ is approximately −0.0052, and its uncertainty must be carefully considered. Also, the correction is sensitive to

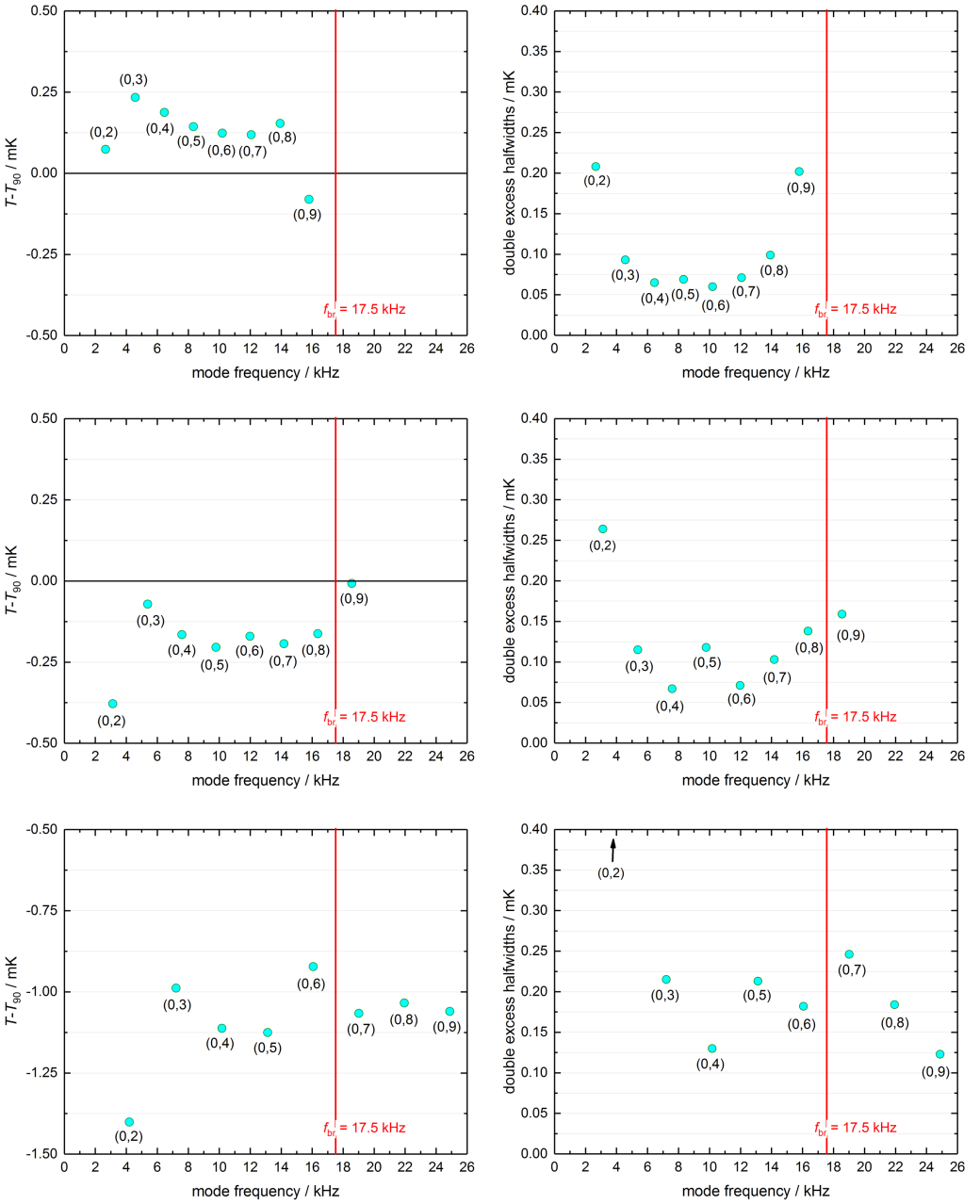

Figure 3. (Left, from top to bottom) Dispersion of $(T-T_{90})$ results determined from eight radial acoustic modes respectively measured at $T_{ref} = T_{90} = 10$ K, 13.8033 K, 24.5561 K. (Right) Double excess halfwidths $2T_{ref}(g_{exp} - g_{calc})/f_{calc}$ scaled in mK units for the same reference temperatures.

errors in the experimental determination of pressure. Based on previous work [7], we conservatively assume ± 25 Pa as a plausible error of our experimental estimate of p and account for its effect on the speed of sound in He with a specific uncertainty contribution (row 4 in table 2). As per equation (1.2), the correction to zero pressure requires estimates of the acoustic (pressure) virial coefficients $\omega_i(T)$ of various order as a function of temperature. Gokul *et al.* [25] recently calculated the terms in the acoustic virial equation of state expanded in terms of density (or pressure as in equation (1.2)), up to the seventh order over the temperature range 2 to 1000 K. These calculations use published information on the density virial coefficients and

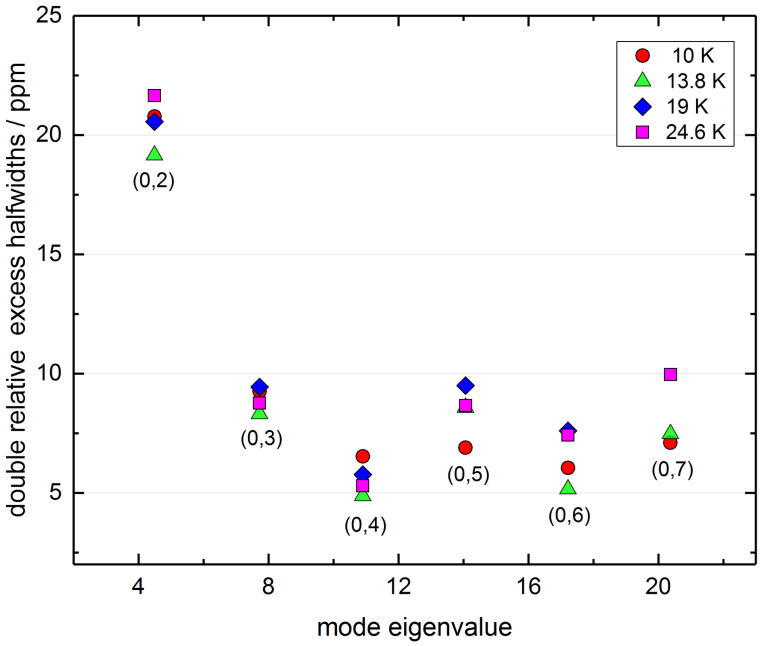

Figure 4. Double relative excess halfwidths $2(g_{exp} - g_{calc})/f_{calc}$ for modes (0,2) to (0,7) at the four temperatures investigated in this work. The datum of mode (0,7) at 19 K is not plotted because strongly perturbed by shell coupling.

the pair and three-body interaction potentials of He [26–29]. Because [26] also reports its own estimates of the second acoustic virial coefficient $\omega_2(T) = \beta_a(T)$, and these are more accurate than in [25], we retain the former source of $\omega_2(T)$ as the most convenient. Otherwise, we assume functions from $\omega_3(T)$ up to $\omega_5(T)$ and their uncertainties from [25] in our implementation of the *ab initio* correction leading from $w_N(T_{ref}, p_{ref})$ to $w_N(T_{ref})$. To exemplify the remarkable accuracy achieved by these calculated properties, note that at 10 K, $\beta_a = -13.546(4)$ cm^3 mol^{-1}, $\omega_3 = 807.0(16)$ cm^6 mol^{-2}, $\omega_4 = 55\,010(37)$ cm^9 mol^{-3} and $\omega_5 = 2.647(6)\times10^{-6}$ cm^{12} mol^{-4}. We use these uncertainties to estimate specific uncertainty contribution to our determinations of T, listed as *ab initio* in row 9 in table 2, relatively spanning between 0.8 ppm and 4.3 ppm for the (T_{ref}, p_{ref}) values investigated here. The right-hand panel in figure 5 plots these relative uncertainty contributions as a function of T for $p = 100$ kPa, showing them decreasing as the uncertainty of the theoretical calculation of $\beta_a(T)$ from [26] decreases significantly at higher temperature. This observation strengthens the validity of an acoustic determination of T based on measurements of the speed of sound in He at a single pressure, instead of the time-consuming procedure of taking several measurements along isotherms. The left-hand plot in figure 5 compares the relative magnitude of successive terms in the acoustic pressure virial expansion in equation (1.2).

Upon correcting to zero pressure, the speed of sound determined for each radial acoustic mode $w_N(T_{ref})$ leads to a determination of the thermodynamic temperature T_N using equation (1.1) and, eventually, to the corresponding determination (T_N–T_{ref}), i.e. to (T_N–T_{90}). The recommended single estimates of (T–T_{90}) listed in table 1 are obtained from the simple arithmetic mean of typically four (out of eight) selected radial modes at each temperature, with the two main criteria for selection (see plots in figures 2 and 3) having small excess halfwidths and not falling close to f_{br} where large shell corrections were applied. Two parameters related to the particular mode selection are considered as main contributions to the uncertainty of T. These are, respectively, the maximum difference in the speed of sound calculated from any of the selected modes (row 5 in table 2), and the mean double excess halfwidth of the selected modes (row 6 in table 2). Note that the alternative calculation of a weighted mean of all the

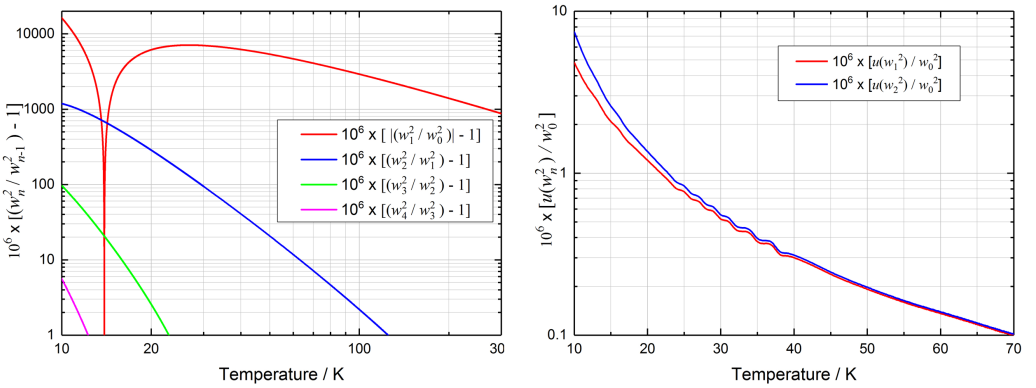

Figure 5. Corrections to squared speed of sound at zero pressure calculated from theory in the temperature range 10 to 300 K. (Left) Relative difference from unity of squared ratios w_n^2/w_{n-1}^2 where w_n^2 are approximations of increasing order in equation (1.2) and $w_1^2 = w_0^2[1+\omega_2(p/RT)]$, $w_2^2 = w_0^2[1+\omega_2(p/RT)+\omega_3(p/RT)^2]$, ... (Right) Relative uncertainty contributions to acoustic determinations of T by *ab initio* corrections of first (up to ω_2) and second order (up to ω_3). In both plots, pressure is fixed at 100 kPa.

eight recorded modes, using excess halfwidths as weights, shifts the final determination of $(T–T_{90})$ by less than 2.5 ppm at all temperatures.

With regard to the traceability to the kilogram required by equation (1.1), i.e. to the need of an accurate, independent estimate of the molar mass of the thermometric gas, we considered the results of three independent mass-spectrometric analyses discussed in [7] for the same bottled source of gas, named L7. These analyses evidenced the presence of trace amounts of Ne and Ar, well below 100 ppb concentration by volume, as the only present impurities, justifying the assumption $\gamma_0 = 5/3$. Below 25 K, the residual concentration of Ar and Ne would be significantly reduced to sublimation pressure over the frozen solid [30]. The same analyses accurately evaluated the ^{3}He/^{4}He isotopic ratio as (0.26 ± 0.08) ppm, leading to the estimate M = 4.0026063 g mol^{-1}, based on the atomic masses of the two He isotopes, with negligible uncertainty.

A summary of the overall uncertainty budget of our determinations of T is listed in table 2, where all the entries are standard uncertainties. There we consider nine distinct sources of uncertainty, separately organized in three categories: (i) acoustic, related to the determination of the acoustic resonance frequencies; (ii) microwave, related to the determination of the cavity radius from microwave frequencies; (iii) *ab initio*, related to the theoretical correction calculated to derive speed of sound at zero pressure from its measured estimates at p_{ref}. All three categories affect the uncertainty of the squared speed of sound, and hence that of the thermodynamic temperature T (with a sensitivity factor of 2), already accounted for in table 2. The combined uncertainties of each category are finally added in quadrature to provide the overall uncertainty of our T determination.

(d) T_{90} calibration and uncertainty

The two types of resistance thermometers carrying T_{90} in the $(T–T_{90})$ determinations were calibrated in distinct ways: CSPRTs by direct realization of cryogenic fixed points (except for VPPs) between 13.8033 and 273.16 K, whereas RIRTs were calibrated by comparisons with a reference national standard RIRT between 4 and 25 K. In general, the latter type of calibration results in a slightly lower confidence, especially when used to give traceability for the CSPRTs to the two VPPs. This results in a measurement uncertainty of ± 0.78 mK (coverage factor k = 1) near 19 K, the largest uncertainty contribution from T_{90} realizations in the present work (see figure 6 and table 3).

CSPRT RS144-01 was previously employed in our RIGT measurements as a north pole thermometer in the same resonator [10], while CSPRT 5435 was the transfer standard of a bilateral comparison carried out between INRiM and LNE-CNAM on different realizations of the scale, obtained by the two metrological institutes in the temperature range 13 to 273 K [2]. Thus, for more detailed information about their characteristics, historical calibration results and individual components of uncertainty, the same considerations already discussed are still valid; a small exception concerns the RS144-01 thermometer, with regard to [10], where only the latest calibration procedure in 2020 was considered because it was closer in time to the measurements presented here. The calibration of 5435 dates back to 2019; however, a stability check performed in 2025 at the triple point of water showed only a very minor increase in the thermometer resistance of a few tens of μΩ after 6 years, corresponding to approximately 0.17 mK. Such a negligible drift reinforces our confidence in the long-term validity of the calibration results and, in particular, with those from LNE-CNAM, at least regarding the ITS-90 realization, given that a very good agreement was found in [2] by means of the transfer standard.

On the other hand, RIRTs 200607 and 200609 were never employed before in a primary thermometry study, neither absolute or relative AGT or RIGT. They were part of a batch of eight thermometers manufactured by Yunnan Dafang™ Meter Industrial Co., Ltd. (former Kunming Dafang Automatic Control Technology Co., Ltd.) tested by Lipinski *et al.* [11] in 2010 from 2.5 to 25 K. RIRTs 200607 and 200609 were selected among the six out of eight thermometers with a stability within ± 1 mK or better at 4.79 K, over 60 thermal cycles down to 4.2 K, and up to approximately 10 K, which also coincides with the lowest bound of the present work. Among the best six RIRTs, 200607 and 200609 were selected as the ones showing the lowest degradation in reproducibility between 10 and 25 K, the full temperature range of this study, quantifiable in ± 0.75 mK for the former and ± 0.5 mK for the latter. More recently in 2017, the RIRTs were calibrated at INRiM by comparison with RIRT 232324, the Italian national standard for the interval between 4 and 25 K. RIRT 232324 carries a 1993 calibration on the NPL-75 scale (the result of the CVGT work by Berry [31]), later converted to an (ICVGT) realization of ITS-90 at INRiM based on local measurements at 4 K, 13.8 K and 24.6 K. RIRT 232324 was used as a reference in the key comparison EURAMET.T-K1 [32] of 2016, alongside INRiM's 2003 results on a CVGT without dead-volume [33,34]. Finally in 2020, it was also used in the bilateral comparison with LNE-CNAM [2] as the only way to provide traceability to the T_{90} VPPs for CSPRTs, thus including 5435 and, previously, RS144-01. All things considered, the measurement standard uncertainty ascribed to both RIRTs in the present work was ± 0.3 mK over the whole temperature range, based on practice and on the assumption that a few thermal cycles would not significantly affect stability and confidence in the final T_{90} calibrations. Regarding the CSPRT RS144-01, we doubt the reliability of the T_{90} determination around 19 K, as no calibration for the two VPPs (contrary to the other fixed points) was repeated after a mechanical shock described in [10]; however, this was compensated for by the very reliable recent results from the 5435 previously outlined. Figure 6 reports the differences in the determination of T_{90} for all the thermometers, at each investigated temperature T, based on the uncertainty contributions discussed above and summarized in table 3. There, the entries in rows 4 and 5 correspond to half of the mean temperature difference between the readings of CSPRTs and RIRTs, respectively. Because the calibration uncertainties of CSPRTs and RIRTs differ significantly at different temperatures, they were used as weights to determine both our initial estimates of T_{exp} and the combined uncertainty of T_{90} listed in table 3.

(e) Determinations of $T–T_{90}$

(i) Single point determinations

The ($T–T_{90}$) determinations listed in table 1 are reproduced in figure 7, where differently coloured uncertainty bars visually distinguish the uncertainty of T from that of T_{90}, showing

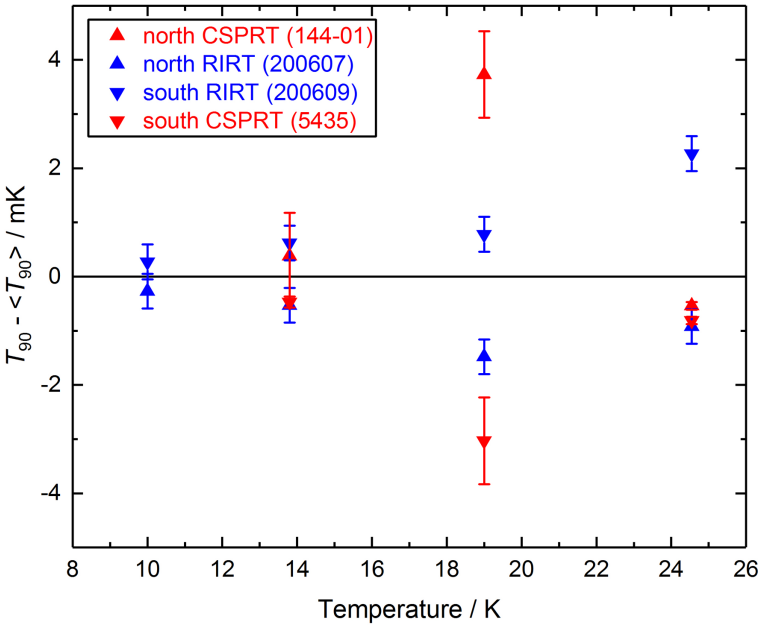

Figure 6. Differences from their mean of the readings of four capsule-type thermometers mounted at different location on the resonant cavity. The set is composed by two RIRTs (blue) and two CSPRTs (red). Up- and down-pointing triangular symbols identify the position of the sensors, respectively near the north or south pole of the cavity. Plotted points and uncertainty bars are based on the T_{90} calibration of the thermometers.

Table 3. Uncertainty budget for the determination of temperature T_{90}.

reference temperature/K		24.5561	19.0000	13.8033	10.0000
reference pressure/kPa		99.98	127.60	91.80	66.64
row	uncertainty source	standard uncertainty $u(T)$/mK			
1	resistance measurement CSPRTs/RIRTs	0.01	0.01	0.01	0.01
2	calibration CSPRTs	0.07	0.78	0.10	NA
3	calibration RIRTs	0.32	0.32	0.32	0.32
4	measurement inconsistency CSPRTs	0.14	3.39	0.43	NA
5	measurement inconsistency RIRTs	1.59	1.13	0.58	0.28
6	combined CSPRTs	0.15	3.47	0.44	NA
7	combined RIRTs	1.62	1.17	0.66	0.42
	weighted mean/mK	**0.22**	**1.51**	**0.46**	**0.42**
		relative standard uncertainty $u_r(T)$/ppm			
	weighted mean/ppm	**8.94**	**79.25**	**33.07**	**42.20**

the former to be significantly smaller than the latter at all temperatures, with the exception of the Ne point, where they have similar magnitude. The Ne point is also an exception regarding the inconsistency between our determination of $(T–T_{90})$ and the recently evaluated consensus estimate [6].

It is of some interest to compare the thermodynamic temperature determination T_{Ne} near the neon point in this work with other obtained by various primary gas thermometry methods over the last two decades [10,15,35–39]. These results, plotted in figure 8 as $(T_{\mathrm{Ne}}- T_{90\mathrm{Ne}})$,

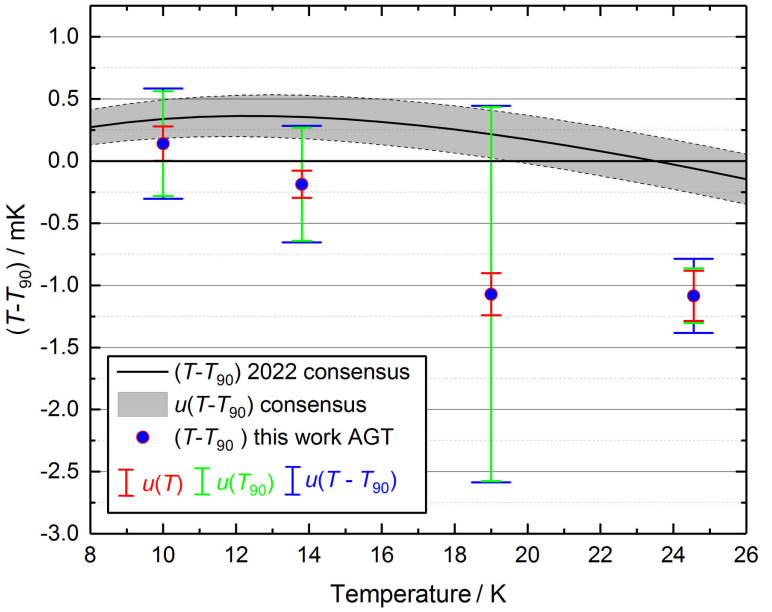

Figure 7. Comparison of the (T–T_{90}) determinations obtained in this work with the interpolating equation developed by Gaiser *et al.* [6] from the consensus estimates on primary thermometry results, updated to 2022, plotted as a black line with the grey shaded area displaying the uncertainty. Differently coloured uncertainty bars refer to the standard uncertainty in the determination of T (red), T_{90} (green), and their combined (T–T_{90}) standard uncertainty (blue).

where T_{90Ne} = 24.5561 K by the ITS-90 definition, all show remarkable agreement within their estimated standard uncertainty $u(T_{Ne})$.

(ii) Multi-point calibration procedure

In addition to the results discussed above, we used our AGT apparatus to perform a measurement run aiming to achieve a *fast*, more complete and informing, thermodynamic calibration of a single temperature sensor (RIRT 200607). The control software was set up to automatically scan the temperature interval from 11.3 K to 26.9 K at several closely spaced (0.4/0.5) K steps, with the corresponding He pressure varying along an isochore from 77 to 185 kPa. With each temperature step lasting 4 h, a total measurement time of 110 h (4.5 days) was required. In the course of the scan, we continuously measured the resonance frequency curve of a single radial acoustic mode (0,4), chosen by reason of its small excess halfwidth and sufficient separation from f_{br} over the whole temperature range. Also, this mode is well isolated in the acoustic spectrum with no close neighbouring non-radial modes, facilitating the software tracing of its resonance curve when the gas temperature suddenly changes at each consecutive step. At these occurrences, the procedure for the acquisition and fit of the resonance curve was sped up by reducing the number of points and the time constant setting on the lock-in analyser. Once that temperature control was fully recovered after each step, an enhanced fitting procedure was used to typically achieve 0.2 ppm precision. From the whole measurement record counting a total of 2500 measurements, approximately 900 were selected for further analysis, with rejection of data points acquired with low-frequency precision or when temperature varied faster than 10 μK min^{-1}. From this record, thermodynamic temperatures were calculated with the same analysis previously described, and then fitted as a function of the corresponding resistance values R_{RIRT} recorded for the thermometer, finding that the calibration function $T(R_{RIRT})$ over the entire temperature range could be adequately represented with an 8th degree polynomial, with the residuals shown in the left-hand plot of figure 9, and a standard deviation of 0.065

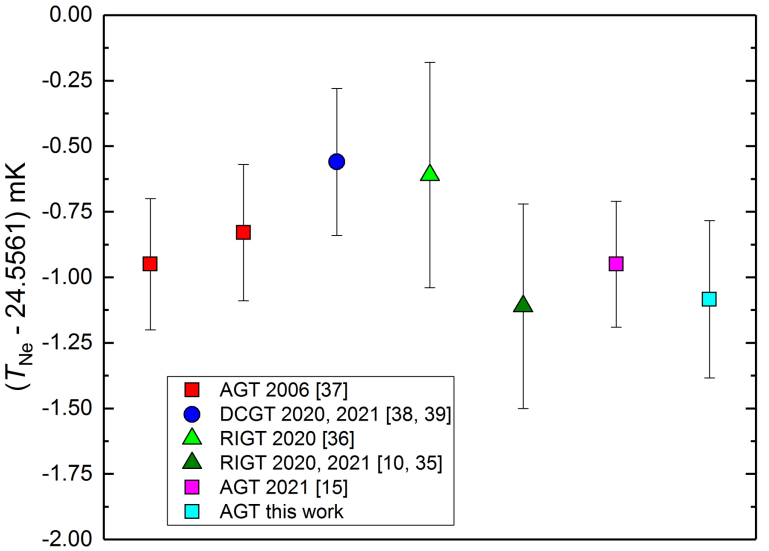

Figure 8. Comparison of thermodynamic temperature determinations near the neon point by different gas thermometry methods.

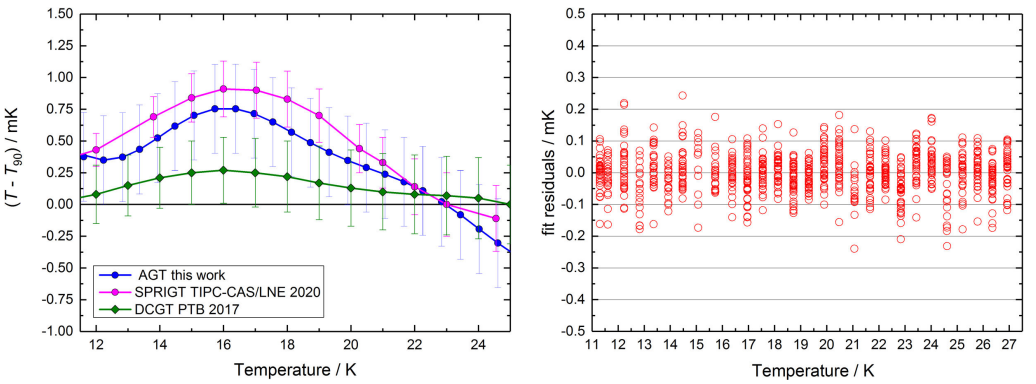

Figure 9. (Left) Residuals from fitting a thermodynamic calibration function in the form of an 8th degree polynomial to the resistance of a RIRT thermometer. (Right) (T–T_{90}) differences from the same calibration compared with other recent determinations with different primary methods [38,40]. The error bars represent standard uncertainties.

mK. From the ITS-90 calibration of the same thermometer, the resulting (T–T_{90}) differences are shown in the right-hand plot of figure 9, where they are compared with other closely spaced determinations obtained with different primary methods, that is, DCGT [38] and single-pressure RIGT [40]. The similarity of the trend of (T–T_{90}) from these three primary thermometry experiments is indeed striking.

4. Conclusions

In this work, we have tested the performance of a simplified AGT primary method for the thermodynamic calibration of capsule-type resistance thermometers as an alternative to the demanding, and time-consuming calibration on ITS-90. The method is simplified by evaluating the speed of sound at zero pressure from measurements at a single pressure, rather than

extrapolating several measurements taken along an isotherm, thus reducing the time needed by a factor of 10. The single-pressure procedure is made possible by the remarkable advances in the calculation of the thermophysical and electromagnetic properties of He. The overall uncertainty achieved with this AGT method is comparable with that achieved with other primary methods and still subject to improvement by future refinements of theoretical models and experimental practice.

Data accessibility. The datasets supporting this article have been uploaded to Zenodo [41].

Supplementary material is available online [42].

Declaration of AI use. We have not used AI-assisted technologies in creating this article.

Authors' contributions. D.I.: data curation, formal analysis, funding acquisition, investigation, methodology, software, supervision, writing—original draft; P.S.: data curation, formal analysis, validation, visualization; R.M.G.: conceptualization, data curation, formal analysis, funding acquisition, investigation, methodology, project administration, resources, software, supervision, writing—original draft.

All authors gave final approval for publication and agreed to be held accountable for the work performed therein.

Conflict of interest declaration. We declare we have no competing interests.

Funding. The project (22IEM02 DireK-T) has received funding from the European Partnership on Metrology, co-financed from the European Union's Horizon Europe Research and Innovation Programme and by the Participating States.

References

1. Preston-Thomas H. 1990 The international temperature scale of 1990 (ITS-90). *Metrologia* **27**, 3–10.
2. Imbraguglio D, Steur PPM, Sparasci F. 2020 Comparison of ITS-90 realizations from 13 K to 273 K between LNE-CNAM and INRIM. *Measurement* **166**, 108225. (doi:10.1016/j.measurement.2020.108225)
3. PokhodunA *et al*. 2021 'Platinum Resistance Thermometry', Guide to the Realization of the ITS-90, 2021, [Online]. See https://www.bipm.org/en/committees/cc/cct/guides-to-thermometry.
4. BIPM. 2019 *The International System of Units (SI Brochure) [9th edition, 2019]*. See https://www.bipm.org/en/publications/si-brochure/.
5. CCT. 2024 *Mise en pratique for the definition of the kelvin in the SI*. See https://www.bipm.org/documents/20126/41489682/SI-App2-kelvin.pdf.
6. Gaiser C *et al*. 2022 Update for the differences between thermodynamic temperature and ITS-90 Below 335 K. *J. Phys. Chem. Ref. Data* **51**, 043105. (doi:10.1063/5.0131026)
7. Gavioso RM, Madonna Ripa D, Steur PPM, Gaiser C, Truong D, Guianvarc'h C, Tarizzo P, Stuart FM, Dematteis R. 2015 A determination of the molar gas constant *R* by acoustic thermometry in helium. *Metrologia* **52**, S274–S304. (doi:10.1088/0026-1394/52/5/s274)
8. Gavioso RM, Benedetto G, Albo PAG, Ripa DM, Merlone A, Guianvarc'h C, Moro F, Cuccaro R. 2010 A determination of the Boltzmann constant from speed of sound measurements in helium at a single thermodynamic state. *Metrologia* **47**, 387–409. (doi:10.1088/0026-1394/47/4/005)
9. Moldover MR, Gavioso RM, Mehl JB, Pitre L, de Podesta M, Zhang JT. 2014 Acoustic gas thermometry. *Metrologia* **51**, R1–R19. (doi:10.1088/0026-1394/51/1/r1)
10. Ripa DM *et al*. 2021 Refractive index gas thermometry between 13.8 K and 161.4 K. *Metrologia* **58**, 025008. (doi:10.1088/1681-7575/abe249)
11. Lipinski L, Szmyrka-Grzebyk A, Lin P, Li XW, Manuszkiewicz H, Jancewicz D, Grykalowska A, Steur PPM, Pavese F. 2010 Development of precision Rh–0.5 at%Fe thermometers of chinese production: further tests. *Int. J. Thermophys.* **31**, 1696–1702. (doi:10.1007/s10765-010-0829-2)
12. Gavioso RM, Madonna Ripa D, Steur PPM, Dematteis R, Imbraguglio D. 2019 Determination of the thermodynamic temperature between 236 K and 430 K from speed of sound measurements in helium. *Metrologia* **56**, 045006. (doi:10.1088/1681-7575/ab29a2)

13. Mehl JB. 2007 Acoustic eigenvalues of a quasispherical resonator: second order shape perturbation theory for arbitrary modes. *J. Res. Natl Inst. Stand. Technol.* **112**, 163. (doi:10.6028/jres.112.013)
14. Garberoglio G *et al*. 2023 *Ab Initio* calculation of fluid properties for precision metrology. *J. Phys. Chem. Ref. Data* **52**, 031502. (doi:10.1063/5.0156293)
15. Pan C *et al*. 2021 Acoustic measurement of the triple point of neon T_{Ne} and thermodynamic calibration of a transfer standard for accurate cryogenic thermometry. *Metrologia* **58**, 045006. (doi:10.1088/1681-7575/ac0711)
16. Gillis KA, Lin H, Moldover MR. 2009 Perturbations from ducts on the modes of acoustic thermometers. *J. Res. Natl Inst. Stand. Technol.* **114**, 263. (doi:10.6028/jres.114.019)
17. Moldover MR, Trusler JPM, Edwards TJ, Mehl JB, Davis RS. 1988 Measurement of the universal gas-constant R using a spherical acoustic resonator. *J. Res. Natl Bur. Stand.* **93**, 85. (doi:10.6028/jres.093.010)
18. Mehl JB. 1985 Spherical acoustic resonator: effects of shell motion. *J. Acoust. Soc. Am.* **78**, 782–788.
19. Puchalski M, Piszczatowski K, Komasa J, Jeziorski B, Szalewicz K. 2016 Theoretical determination of the polarizability dispersion and the refractive index of helium. *Phys. Rev.* **93**, 032515. (doi:10.1103/physreva.93.032515)
20. Garberoglio G, Harvey AH. 2020 Path-integral calculation of the second dielectric and refractivity virial coefficients of helium, neon, and argon. *J. Res. Natl Inst. Stand. Technol.* **125**, 125022. (doi:10.6028/jres.125.022)
21. Garberoglio G, Harvey AH, Jeziorski B. 2021 Path-integral calculation of the third dielectric virial coefficient of noble gases. *J. Chem. Phys.* **155**, 234103. (doi:10.1063/5.0077684)
22. Puchalski M, Lesiuk M, Jeziorski B. 2023 Relativistic treatment of the diamagnetic susceptibility of helium. *Phys. Rev.* **108**, 042812. (doi:10.1103/physreva.108.042812)
23. Mehl JB. 2015 Second-order electromagnetic eigenfrequencies of a triaxial ellipsoid II. *Metrologia* **52**, S227–S232. (doi:10.1088/0026-1394/52/5/s227)
24. Underwood RJ, Mehl JB, Pitre L, Edwards G, Sutton G, de Podesta M. 2010 Waveguide effects on quasispherical microwave cavity resonators. *Meas. Sci. Technol.* **21**, 075103. (doi:10.1088/0957-0233/21/7/075103)
25. Gokul N, Schultz AJ, Kofke DA. 2021 Speed of sound in helium-4 from Ab Initio acoustic virial coefficients. *J. Chem. Eng. Data* **66**, 3258–3281. (doi:10.1021/acs.jced.1c00328)
26. Czachorowski P, Przybytek M, Lesiuk M, Puchalski M, Jeziorski B. 2020 Second virial coefficients for He 4 and He 3 from an accurate relativistic interaction potential. *Phys. Rev. A* **102**, 042810. (doi:10.1103/PhysRevA.102.042810)
27. Schultz AJ, Kofke DA. 2019 Virial coefficients of helium-4 from *Ab Initio* -based molecular models. *J. Chem. Eng. Data* **64**, 3742–3754. (doi:10.1021/acs.jced.9b00183)
28. Przybytek M, Cencek W, Komasa J, Łach G, Jeziorski B, Szalewicz K. 2012 Erratum: relativistic and quantum electrodynamics effects in the helium pair potential. *Phys. Rev. Lett.* **104**, 183003. (doi:10.1103/PhysRevLett.104.183003)
29. Cencek W, Patkowski K, Szalewicz K. 2009 Full-configuration-interaction calculation of three-body nonadditive contribution to helium interaction potential. *J. Chem. Phys.* **131**, 064105. (doi:10.1063/1.3204319)
30. Lemmon EW, Bell IH, Huber ML, McLinden MO. 2018 *NIST standard reference database 23: reference fluid thermodynamic and transport properties-refprop, version 10.0*. Gaithersburg, MD, USA: National Institute of Standards and Technology, Standard Reference Data Program.
31. Berry KH. 1979 NPL-75: a low temperature gas thermometry scale from 2.6 K to 27.1 K. *Metrologia* **15**, 89–115. (doi:10.1088/0026-1394/15/2/006)
32. Gaiser C, Fellmuth B, Steur P, Szmyrka-Grzebyk A, Manuszkiewicz H, Lipinski L, Peruzzi A, Rusby R, Head D. 2017 EURAMET key comparison no. EURAMET.T-K1: realisations of the ITS-90 from 2.6 K to 24.5561 K, using rhodium-iron resistance thermometers. *Metrologia* **54**, 03002. (doi:10.1088/0026-1394/54/1a/03002)
33. Steur PPM. 2003 The IMGC interpolating constant volume gas thermometer — new data. In *AIP Conference Proceedings*. Chicago, IL, USA. (doi:10.1063/1.1627112)
34. Steur PPM, Giraudi D. 2013 *Adjustments to the ICVGT scale of inrim*, pp. 124–129. Los Angeles, CA, USA. See https://pubs.aip.org/aip/acp/article/1552/1/124-129/878530.

35. Ripa DM *et al*. 2021 Corrigendum: refractive index gas thermometry between 13.8 K and 161.4 K. *Metrologia* **58**, 069501. (doi:10.1088/1681-7575/ac2d9e)
36. Rourke PMC. 2020 Thermodynamic temperature of the triple point of xenon measured by refractive index gas thermometry. *Metrologia* **57**, 024001. (doi:10.1088/1681-7575/ab57f2)
37. Pitre L, Moldover MR, Tew WL. 2006 Acoustic thermometry: new results from 273 K to 77 K and progress towards 4 K. *Metrologia* **43**, 142–162. (doi:10.1088/0026-1394/43/1/020)
38. Gaiser C, Fellmuth B, Haft N. 2017 Primary thermometry from 2.5 K to 140 K applying dielectric-constant gas thermometry. *Metrologia* **54**, 141–147. (doi:10.1088/1681-7575/aa5389)
39. Gaiser C, Fellmuth B. 2021 Primary thermometry at 4 K, 14 K, and 25 K applying dielectric-constant gas thermometry. *Metrologia* **58**, 042101. (doi:10.1088/1681-7575/ac0d4a)
40. Gao B *et al*. 2021 Corrigendum: measurement of thermodynamic temperature between 5 K and 24.5 K with single-pressure refractive-index gas thermometry. *Metrologia* **58**, 059501. (doi:10.1088/1681-7575/ac1e04)
41. Imbraguglio D. 2025 Data for: Direct calibration of resistance thermometers between 10 K and 25 K by absolute acoustic gas thermometry in helium. Zenodo. (doi:10.5281/zenodo.17508803)
42. Imbraguglio D, Steur P, Gavioso RM. 2025 Supplementary material from: Direct calibration of resistance thermometers between 10 K and 25 K by absolute acoustic gas thermometry in helium. Figshare. (doi:10.6084/m9.figshare.c.8153723)